GEOPHYSICS, VOL. 78, NO. 6 (NOVEMBER-DECEMBER 2013); P. N35–N42, 9 FIGS., 1 TABLE.
10.1190/GEO2012-0529.1

Downloaded 01/25/15 to 121.251.241.147. Redistribution subject to SEG license or copyright; see Terms of Use at http://library.seg.org/

Elastic impedance parameterization and inversion with Young's modulus and Poisson's ratio

Zhaoyun Zong[1], Xingyao Yin[1], and Guochen Wu[1]

ABSTRACT

Young's modulus and Poisson's ratio are related to quantitative reservoir properties such as porosity, rock strength, mineral and total organic carbon content, and they can be used to infer preferential drilling locations or sweet spots. Conventionally, they are computed and estimated with a rock physics law in terms of P-wave, S-wave impedances/velocities, and density which may be directly inverted with prestack seismic data. However, the density term imbedded in Young's modulus is difficult to estimate because it is less sensitive to seismic-amplitude variations, and the indirect way can create more uncertainty for the estimation of Young's modulus and Poisson's ratio. This study combines the elastic impedance equation in terms of Young's modulus and Poisson's ratio and elastic impedance variation with incident angle inversion to produce a stable and direct way to estimate the Young's modulus and Poisson's ratio, with no need for density information from prestack seismic data. We initially derive a novel elastic impedance equation in terms of Young's modulus and Poisson's ratio. And then, to enhance the estimation stability, we develop the elastic impedance varying with incident angle inversion with damping singular value decomposition (EVA-DSVD) method to estimate the Young's modulus and Poisson's ratio. This method is implemented in a two-step inversion: Elastic impedance inversion and parameter estimation. The introduction of a model constraint and DSVD algorithm in parameter estimation renders the EVA-DSVD inversion more stable. Tests on synthetic data show that the Young's modulus and Poisson's ratio are still estimated reasonable with moderate noise. A test on a real data set shows that the estimated results are in good agreement with the results of well interpretation.

INTRODUCTION

Rock brittleness plays an important role in evaluation of hydraulic fracturing for unconventional reservoirs. Young's modulus and Poisson's ratio are related to quantitative reservoir properties such as porosity, rock strength, mineral and total organic carbon content, and they can be used for rock brittleness evaluation and to infer preferential drilling locations or sweet spots (Harris et al., 2011; Sena et al., 2011). With seismic data, Young's modulus and Poisson's ratio are conventionally computed indirectly from P-wave, S-wave impedances/velocities, and density which can be inverted from seismic data directly (Sena et al., 2011), as shown in Goodway et al. (1997). However, it contains two challenges. On the one hand, the density imbedded in the Young's modulus is difficult to invert. Downton (2005) points out that large angles of incidence and large offsets are needed to determine density and the estimated density reflectivity shows more bias than the P-impedance and S-impedance reflectivities when noise exists, i.e., the estimated density is more contaminated by noise than the estimated P-impedance reflectivity and S-impedance reflectivity, even with large incident angles. On the other hand, the indirect way of parameters estimation can create more uncertainty caused by the indirect calculation (Wang et al., 2006; Zhang et al., 2009). As shown in Wang et al. (2006), compared with the direct way to estimate the Lamé parameters from prestack seismic data, the indirect way of Lamé parameters estimation from the inverted P-wave and S-wave information causes much more bias. In this paper, we will present a direct approach to estimate Young's modulus and Poisson's ratio to avoid the uncertain density and accumulated error from indirect calculation.

Elastic impedance (EI) inversion has been widely studied in literature. Connolly (1999) initially formulated the EI equation and introduced the concept of EI in terms of P-wave, S-wave velocity,

Manuscript received by the Editor 18 December 2012; revised manuscript received 8 May 2013; published online 3 October 2013.
[1]China University of Petroleum (Huadong), Qingdao, Shandong, China. E-mail: zhaoyunzong@yahoo.com; xyyin@upc.edu.cn; guochenwu@upc.edu.cn.
© 2013 Society of Exploration Geophysicists. All rights reserved.

Downloaded 01/25/15 to 121.251.241.147. Redistribution subject to SEG license or copyright; see Terms of Use at http://library.seg.org/

and density, where angle stacks for a range of incidence angles of prestack seismic data are inverted based on this novel concept. Cambois et al. (2000) implement the estimation of P-wave, S-wave velocity and density from elastic impedances, and show that elastic impedance inversion mainly contains two steps: first to invert angle-limited stacks under the constraint of simulated logs, and then to extract the desired elastic parameters. He also shows that, compared with AVO inversion, the elastic impedance inversion can avoid the attributes "leakage" caused by wavelets in different offsets or incident angles. The robust wavelet stripping in EI inversion and the ability of discriminating lithology or even fluid with estimated elastic impedances in some angle makes it widely used in industry (Whitcombe, 2002; Arsalan and Yadav, 2009; Thompson et al., 2009). Whitcombe et al. (2002) propose a normalized EI equation to deal with the dimensionality problem.

The definition of elastic impedance has also been extended in different media or parameterization. Duffaut et al. (2000) define the shear elastic impedance and consider that the joint P-P and P-S elastic impedance inversion may provide a more stable way to estimate the ratio of P-wave velocity and S-wave velocity. Savic et al. (2000) define the elastic impedance as the function of P-wave, S-wave velocities and ray parameters to deal with the dimensionality problem. Martins (2002) defines the elastic in weak anisotropic media, Ma and Morozov (2005, 2006) study the generalized and Zoeppritz EI. Beside, using a different parameterization, Wang et al. (2006) define the elastic impedance in terms of Lamé parameters, and Zhang et al. (2009) define the elastic impedance in term of fluid/pore term as discussed in Russell et al. (2003), and they show that, comparing with indirect way, the direct extraction is much more reasonable. Details about the development of elastic impedance can also be found in Morozov (2010).

There are two main steps for parameters estimation with the elastic impedance equation; elastic impedance inversion, and parameters extraction from elastic impedances. The elastic impedances in different incident angle range can be estimated reasonably with a conventional poststack seismic inversion algorithm, such as constrained sparse spike inversion (CSSI) or model-based inversion algorithm. However, the method to estimate the elastic parameters from elastic impedances is still challenging. Cambois et al. (2000) state that it is possible to estimate the elastic parameters from elastic impedances with a linear fit algorithm. However, Mallick et al. (2000, 2007) show that, in the presence of 2% random noise, this method displays dramatic instability to extract three parameters from synthetic data, which has also been confirmed by Lu et al. (2004). On the basis of previous studies, our current study proposes and implements the practical elastic impedance varying with incident angle inversion with a damped singular value decomposition (EVA-DSVD) method, based on a novel elastic impedance equation in terms of Young's modulus and Poisson's ratio. Two steps are contained in the proposed method. We use the seismic inversion algorithm in a Bayesian scheme to implement the elastic impedance inversion (Zong et al., 2011), and the Young's modulus and Poisson's ratio are extracted from elastic impedances in a model constrained method with a damped singular value decomposition algorithm in the inversion scheme. The proposed EVA-DSVD inversion method renders the parameter estimation from elastic impedances more stable. We will initially derive the novel elastic impedance equation and give the form of its normalization, and then discuss the EVA-DSVD method. We end with model and real data case studies that illustrate the method.

ELASTIC IMPEDANCE PARAMETERIZATION WITH YOUNG'S MODULUS AND POISSON'S RATIO

Under the assumption that only small relative changes in elastic parameters occur across the welded elastic interface, the linearized P-wave reflection coefficient for an incident P-wave as a function of angle can be approximated with different types of model parameterizations. Bortfeld initially gives the linearized P-wave reflection coefficient equation in terms of P-wave, S-wave velocities and density, and this kind of parameterization has also been discussed in different form (Aki and Richards, 1980). Fatti et al. (1994) study the linearized P-wave reflection coefficient equation in terms of P-wave, S-wave impedances, and density, which is considered to be more stable in AVO inversion (Downton, 2005). Shuey (1985) studies the approximate P-wave reflection coefficient equation in terms of Poisson ratio, P-wave velocity, and density, and it shows great potential in AVO analysis. However, the nonlinearity of this approximation limits its application in AVO inversion. To discuss the fluid factor estimation from prestack seismic data, Goodway et al. (1997) discuss the linearized P-wave reflection coefficient equation in terms of Lamé parameters and Russell et al. (2011) discuss the equation in term of pore/fluid factor. Beside, Zong et al. (2012) present the linearized P-wave reflection coefficient equation in terms of P-wave, S-wave moduli, and density as

$$R(\theta) = \frac{1}{4}\sec^2\theta\frac{\Delta M}{M} - 2\left(\frac{\beta}{\alpha}\right)^2\sin^2\theta\frac{\Delta\mu}{\mu} + \left(\frac{1}{2} - \frac{1}{4}\sec^2\theta\right)\frac{\Delta\rho}{\rho}, \quad (1)$$

where α is average P-wave velocity of upper and lower medium, β is the average S-wave velocity of upper and lower medium, θ is the incident angle, $\Delta M/M$ is P-wave modulus reflectivity, $\Delta\mu/\mu$ is S-wave modulus reflectivity, $\Delta\rho/\rho$ is density reflectivity, and they can be expressed as

$$\frac{\Delta M}{M} = \frac{2(M_1 - M_2)}{(M_1 + M_2)}, \quad (2)$$

$$\frac{\Delta\mu}{\mu} = \frac{2(\mu_1 - \mu_2)}{(\mu_1 + \mu_2)}, \quad (3)$$

$$\frac{\Delta\rho}{\rho} = \frac{2(\rho_1 - \rho_2)}{(\rho_1 + \rho_2)}, \quad (4)$$

here $M_1, M_2, \mu_1, \mu_2, \rho_1$, and ρ_2 are the related parameters in the media touching at the reflector.

The relationships among P-wave modulus reflectivity, S-wave modulus reflectivity, Poisson's ratio, Young's modulus, and density reflectivity are shown below:

Downloaded 01/25/15 to 121.251.241.147. Redistribution subject to SEG license or copyright; see Terms of Use at http://library.seg.org/

$$\frac{\Delta M}{M} = \frac{\Delta E}{E} + \left(\frac{\sigma}{(2\sigma-1)(\sigma-1)} - \frac{\sigma}{1+\sigma}\right)\frac{\Delta\sigma}{\sigma}, \quad (5)$$

$$\frac{\Delta\mu}{\mu} = \frac{\Delta E}{E} - \frac{\sigma}{1+\sigma}\frac{\Delta\sigma}{\sigma}, \quad (6)$$

where

$$\sigma = \frac{1-2k}{2-2k}, \qquad k = \frac{\beta^2}{\alpha^2}. \quad (7)$$

Substituting equations 5–7 into equation 1, yields

$$R(\theta) = a(\theta)\frac{\Delta E}{E} + b(\theta)\frac{\Delta\sigma}{\sigma} + c(\theta)\frac{\Delta\rho}{\rho}, \quad (8)$$

where

$$a(\theta) = \frac{1}{4}\sec^2\theta - 2k\sin^2\theta, \quad (9)$$

$$b(\theta) = \frac{1}{4}\sec^2\theta\frac{(2k-3)(2k-1)^2}{k(4k-3)} + 2k\sin^2\theta\frac{1-2k}{3-4k}, \quad (10)$$

$$c(\theta) = \frac{1}{2} - \frac{1}{4}\sec^2\theta. \quad (11)$$

Equation 8 establishes the relationship among P-wave reflectivity and Young's modulus, Poisson's ratio and density directly, and it will be called the *YPD equation*.

Following the conception of elastic impedance of Connolly (1999), the reflectivity can also be defined as

$$R(\theta) \asymp \frac{1}{2}\frac{\Delta \mathrm{EI}}{\overline{\mathrm{EI}}} \asymp \frac{1}{2}\Delta\ \ln(\mathrm{EI}), \quad (12)$$

where EI is the elastic impedance. Substituting equation 12 into equation 11, yields

$$\Delta\ \ln(\mathrm{EI}) = a(\theta)\frac{\Delta E}{E} + b(\theta)\frac{\Delta\sigma}{\sigma} + c(\theta)\frac{\Delta\rho}{\rho}. \quad (13)$$

After some algebraic operation, equation 13 yields

$$\mathrm{EI}(\theta) = E^{a(\theta)}\sigma^{b(\theta)}\rho^{c(\theta)}. \quad (14)$$

Following the normalization method proposed by Whitecombe, equation 14 can be normalized to deal with the dimensional problem as

$$\mathrm{EI}(\theta) = A_0\left(\frac{E}{E_0}\right)^{a(\theta)}\left(\frac{\sigma}{\sigma_0}\right)^{b(\theta)}\left(\frac{\rho}{\rho_0}\right)^{c(\theta)}, \quad (15)$$

where A_0, E_0, σ_0, and ρ_0 is the statistic average of elastic impedance, Young's modulus, Poisson's ratio, and density, respectively. They can be estimated from well log curves. This equation is the elastic impedance equation in terms of Young's modulus, Poisson's ratio, and density.

To test the accuracy of the novel elastic impedance equation 14, we substitute equation 14 or 15 into equation 12 to estimate the reflection coefficients (named as YPD-EI in Figure 1) of a three-layer model modified from Goodway et al. (1997). The P-wave velocities, S-wave velocities, and densities of the model in the upper media are displayed in Table 1. This model contains two kinds of reflectors: the first two layers with negative impedance reflector (the impedance in upper medium is larger than that in lower medium) and the last two layers with positive impedance reflector (the impedance in upper medium is smaller than that in lower medium). We compare YPD-EI with the reflection coefficients estimated from exact Zoeppritz equation, Aki-Richard approximate equation (Aki in Figure 1) and equation 8 (YPD in Figure 1), respectively. Figure 1a displays the reflection coefficients with the exact Zoeppritz

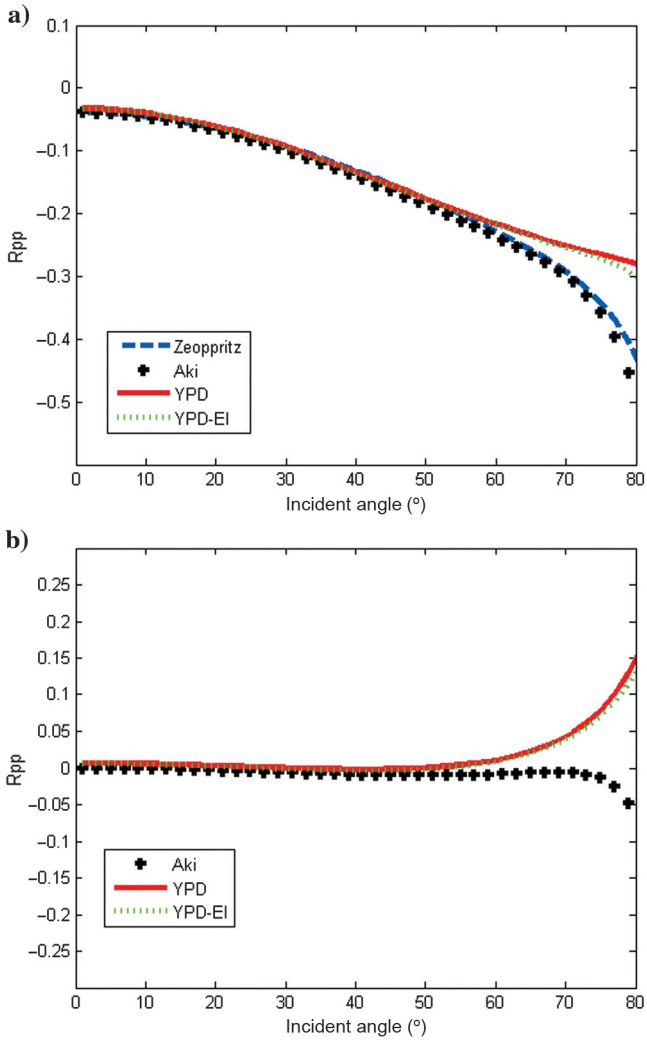

Figure 1. Comparison of exact Zoeppritz equation, Aki-Richard approximate equation, YPD equation, and YPD-EI of the negative reflector. (a) Reflection coefficients with exact Zoeppritz equation, Aki-Richard approximate equation, YPD equation, and YPD-EI (b) Difference of reflection coefficients from the exact Zoeppritz equation and Aki-Richard approximate equation, YPD equation, and YPD-EI.

Downloaded 01/25/15 to 121.251.241.147. Redistribution subject to SEG license or copyright; see Terms of Use at http://library.seg.org/

equation, Aki-Richard approximate equation, YPD, and YPD-EI of negative impedance reflector, Figure 1b displays the difference of reflection coefficients of approximate equations from the exact Zoeppritz equation of negative impedance reflector. Figure 2a and 2b display the related reflection coefficients and reflection coefficients difference of positive reflector. Note from Figures 1 and 2 that the reflection coefficient combining equations 14 and 12 (YPD-EI) is close to the modeling result from Aki-Richard approximate equation and the exact Zoeppritz equation until the incident angle reaches 50°.

ELASTIC IMPEDANCE INVERSION FOR YOUNG'S MODULUS AND POISSON'S RATIO

There are two steps for Young's modulus and Poisson's ratio estimation with the proposed elastic impedance equation 15: elastic impedance inversion and Young's modulus and Poisson's ratio extraction from elastic impedances.

Elastic impedance inversion is generally implemented combining angle-stack seismic data with the corresponding wavelet. The inversion algorithm is the same as that in poststack seismic inversion. In this paper, we use the elastic impedance inversion in Bayesian scheme proposed by Zong et al. (2011) to estimate the elastic impedances in the angle domain for selected angles. This method uses a Cauchy probability distribution as the prior probability distribution, which will lead to a high-resolution result (Sacchi and Ulrych, 1995; Alemie and Sacchi, 2011). We will initially introduce the elastic Bayesian inversion briefly.

Gaussian and Cauchy probability distributions are used for the likelihood function $p(\mathbf{d}|\mathbf{m})$ and the elastic impedance reflection coefficient $\mathbf{m}$. The post probability distribution $p(\mathbf{m}|\mathbf{d})$ can be expressed as

$$p(\mathbf{m}|\mathbf{d}) \propto \prod_{i=1}^{M}\left[\frac{1}{1+m_i^2/\sigma_m^2}\right]\cdot\exp\left[-\frac{(\mathbf{Gm}-\mathbf{d})^{\mathrm{T}}(\mathbf{Gm}-\mathbf{d})}{2\sigma_n^2}\right], \tag{16}$$

where $\mathbf{d}$ is the angle-stack seismic data as data vector, σ_n^2 is noise covariance, $\mathbf{G}$ is wavelet matrix, T is the transpose of matrix, and σ_m^2 is covariance of model vector $\mathbf{m}$. Maximizing equation 16, and combining the model constraint (Zong et al., 2011), the target function $F(\mathbf{m})$ becomes

$$F(\mathbf{m}) = F_{\mathbf{G}}(\mathbf{m}) + F_C(\mathbf{m}) + F_E(\mathbf{m}). \tag{17}$$

Three parts are included in equation 17: $F_G(\mathbf{m})$ represents the difference between modeling and observed data, resulting from likelihood; $F_C(\mathbf{m})$ represents the prior Cauchy distribution constraints; and $F_E(\mathbf{m})$ represents the model constraint. Combining with the optimization solution from equation 17, the elastic impedance is equated to a time integration followed by an exponentiation.

Young's modulus and Poisson's ratio extraction from elastic impedances is implemented in an inversion scheme named elastic impedance varying with incident angle with damped singular value decomposition (EVA-DSVD).

Taking the logarithm on both sides of equation 15 and after some algebraic operation, the result is

$$\ln\frac{\mathrm{EI}(\theta)}{A_0} = a(\theta)\ln\left(\frac{E}{E_0}\right) + b(\theta)\ln\left(\frac{\sigma}{\sigma_0}\right) + c(\theta)\ln\left(\frac{\rho}{\rho_0}\right). \tag{18}$$

Table 1. Model for gas-bearing sand and shale modified from Goodway (1997).

Parameters	V_p(m/s)	V_s(m/s)	ρ(g/cm^2)	σ	V_p/V_s
Shale	2898	1290	2.425	0.38	2.25
Gas-bearing sand	2857	1666	2.275	0.24	1.71
Shale	2898	1290	2.425	0.38	2.25

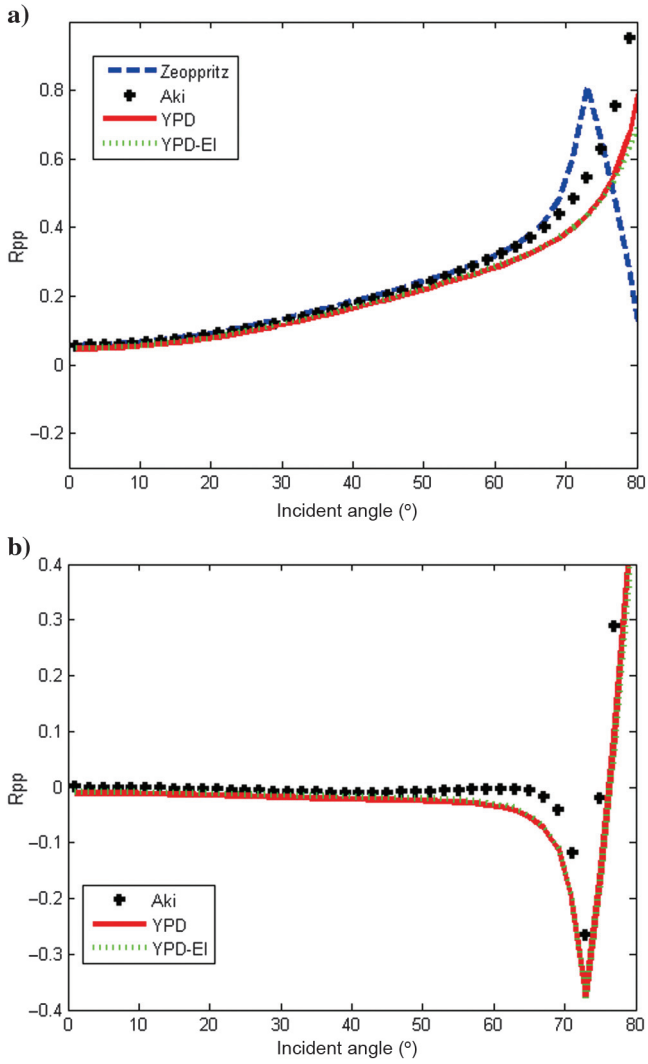

Figure 2. Comparison of exact Zoeppritz equation, Aki-Richard approximate equation, YPD equation, and YPD-EI of the positive reflector. (a) Reflection coefficients with exact Zoeppritz equation, Aki-Richard approximate equation, YPD equation, and YPD-EI (b) Difference of reflection coefficients from the exact Zoeppritz equation and Aki-Richard approximate equation, YPD equation, and YPD-EI.

Downloaded 01/25/15 to 121.251.241.147. Redistribution subject to SEG license or copyright; see Terms of Use at http://library.seg.org/

Defining

$$L_e = \ln \frac{EI(\theta)}{A_0}, \tag{19}$$

$$L_E = \ln\left(\frac{E}{E_0}\right), \tag{20}$$

$$L_\sigma = \ln\left(\frac{\sigma}{\sigma_0}\right), \tag{21}$$

$$L_\rho = \ln\left(\frac{\rho}{\rho_0}\right). \tag{22}$$

If the number of angles is M, and a trace contains N samples, substituting equation 19–22 into equation 18, yields

$$\begin{bmatrix} \bar{L}_{e1} \\ \bar{L}_{e2} \\ \vdots \\ \bar{L}_{eM} \end{bmatrix} = \begin{bmatrix} \bar{A}_1 & \bar{B}_1 & \bar{C}_1 \\ \bar{A}_2 & \bar{B}_2 & \bar{C}_2 \\ & \cdots & \\ \bar{A}_M & \bar{B}_M & \bar{C}_M \end{bmatrix} \begin{bmatrix} \bar{L}_E \\ \bar{L}_\sigma \\ \bar{L}_\rho \end{bmatrix}, \tag{23}$$

where

$$\bar{L}_{e1} = [\, L_{e1}^1 \quad \ldots \quad L_{e1}^N \,]^T, \tag{24}$$

$$\bar{A}_1 = \mathrm{diag}[\, a_1^1 \quad \ldots \quad a_1^N \,], \tag{25}$$

$$\begin{aligned} \bar{L}_E &= [\, L_E^1 \quad \ldots \quad L_E^N \,]^T \\ \bar{L}_\sigma &= [\, L_\sigma^1 \quad \ldots \quad L_\sigma^N \,]^T \\ \bar{L}_\rho &= [\, L_\rho^1 \quad \ldots \quad L_\rho^N \,]^T. \end{aligned} \tag{26}$$

Equation 23 can be written as

$$\mathbf{D} = \bar{\mathbf{G}}'\bar{\mathbf{R}}'. \tag{27}$$

To enhance the resolution in solving equation 27, the Cauchy constraint can be utilized for equation 27 as

$$F(\bar{\mathbf{R}}') = (\mathbf{D} - \bar{\mathbf{G}}'\bar{\mathbf{R}}')^{\mathrm{T}}(\mathbf{D} - \bar{\mathbf{G}}'\bar{\mathbf{R}}') + \lambda \sum_{i=1}^{M} \ln(1 + \bar{R}_i'^2). \tag{28}$$

Minimizing the target function 28 and combining with the model constraint yields

$$\mathbf{\Psi} = \mathbf{K}\mathbf{\Phi}, \tag{29}$$

where

$$\mathbf{\Psi} = \bar{\mathbf{G}}'^{\mathrm{T}}\mathbf{D} + \mathbf{P}_E^T\eta_E + \mathbf{P}_\sigma^T\eta_\sigma + \mathbf{P}_\rho^T\eta_\rho, \tag{30}$$

$$\mathbf{K} = \bar{\mathbf{G}}'^{T}\bar{\mathbf{G}}' + \lambda_c\mathbf{Q} + \lambda_E\mathbf{P}_E^T\mathbf{P}_E + \lambda_\sigma\mathbf{P}_\sigma^T\mathbf{P}_\sigma + \lambda_\rho\mathbf{P}_\rho^T\mathbf{P}_\rho, \tag{31}$$

$$\mathbf{\Phi} = \bar{\mathbf{R}}', \tag{32}$$

$$\boldsymbol{\eta}_i = 1/2 * \ln(\mathbf{L}_i/\mathbf{L}_{i0})_i, i = E, \sigma, \rho, \tag{33}$$

and $\lambda_i, i = E, \sigma, \rho$ is the constraint coefficients of Young's modulus, Poisson's ratio and density.

To enhance the stability in solving equation 29, the damped singular value decomposition algorithm is introduced. The generalized inverse of $\mathbf{K}$ is

$$\mathbf{K}_g^{-1} = \mathbf{V}\mathbf{\Lambda}(\mathbf{\Lambda}_p^2 + \varepsilon^2\mathbf{I})^{-1}\mathbf{U}^T, \tag{34}$$

and then, the estimation for $\mathbf{\Phi}$ is

$$\mathbf{\Phi}^{\mathrm{est}} = \mathbf{V}\mathbf{\Lambda}(\mathbf{\Lambda}_p^2 + \varepsilon^2\mathbf{I})^{-1}\mathbf{U}^T\mathbf{\Psi}. \tag{35}$$

With the estimated $\mathbf{\Phi}^{\mathrm{est}}$, combining with equation 20–22, we can estimate the Young's modulus, Poisson's ratio, and density.

EXAMPLES

Synthetic test

We test the EVA-DSVD inversion method on a synthetic earth profile from real well logs. Figure 3 shows original (in blue), initial (in green), and inverted (in red) Young's modulus, Poisson ratio, and density of well A with different signal-to-noise ratio (S/N). S/N is the ratio between the root mean square amplitude of the signal and the root mean square amplitude of the noise, with the noise normally distributed. The initial models are obtained by smoothing the original models. We perform the inversion with equation 15. From Figure 3a, we see that all the parameters can be inverted well when there is no noise in the synthetic data and with rather smooth initial Young's modulus, Poisson ratio, and density. To test the stability of the inversion method, we add random Gaussian noise to the synthetic traces, with different S/N, and the S/N is 5:1 and 2:1, respectively. It is easy to demonstrate that the Young's modulus can be estimated well even in the case with an S/N of 2:1, and the Poisson ratio and density can also be estimated reasonably, however, the density shows more bias from the true value.

Real data example

Real data is used to validate the application of the proposed EVA-DSVD prestack seismic inversion method. True-amplitude processing has been implemented before inversion of the real data. The seismic data was processed by a contractor and the processing sequence was defined to ensure that the final prestack amplitudes should image the reflection strength of the subsurface interfaces as correctly as possible. We assume that wave mode conversions, interbed multiples, and anisotropy effects can be neglected after processing. Three partial angle-stack seismic profiles are shown in Figure 4. The maximum incident angle is around 35°. The target reservoir is circled as a black ellipse as shown in each profile,

Downloaded 01/25/15 to 121.251.241.147. Redistribution subject to SEG license or copyright; see Terms of Use at http://library.seg.org/

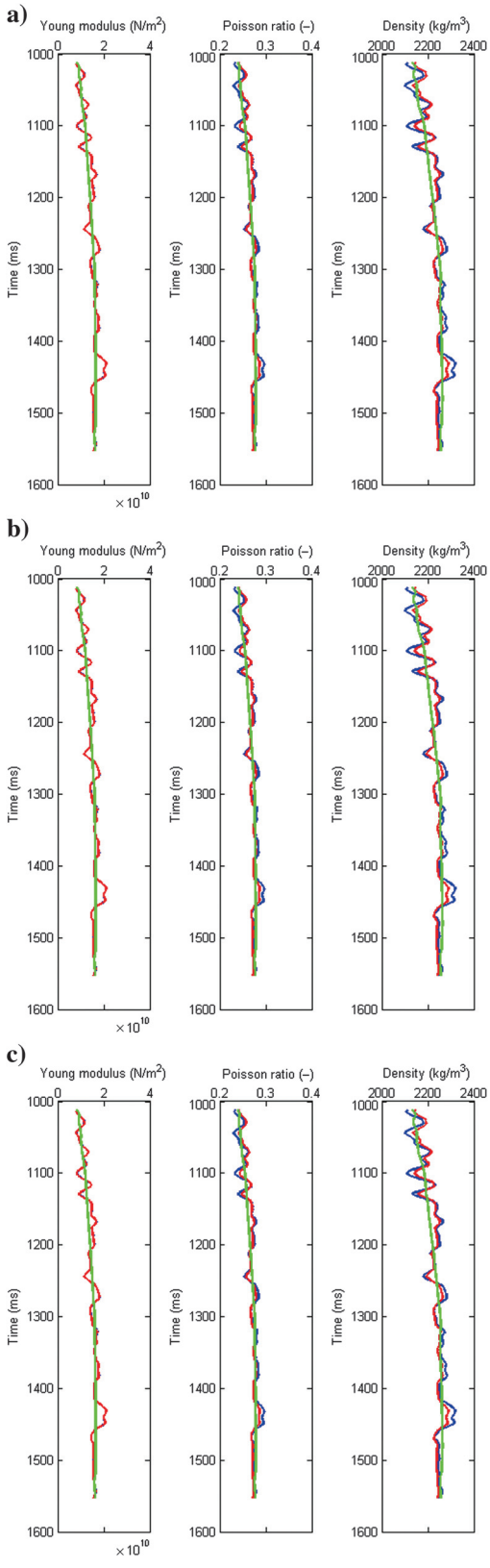

Figure 3. Model inversion result with different noise (red means inversion result, blue means original model, green means initial model). (a) No noise, (b) S/N = 5, (c) S/N = 2.

respectively, and the black line in Figure 4a sketches the bore path of the known well. The estimated elastic impedances of each angle using elastic Bayesian inversion as discussed in this paper are displayed in Figure 5. From Figure 5, we can see that the elastic impedances at each angle all show an anomalously high value in the target reservoir. Furthermore, we implement the proposed EVA-DSVD method with the estimated elastic impedances. The inverted results of Young's modulus, Poisson ratio, and density with smooth initial models are displayed in Figures 6–8, respectively. Figure 9 shows the comparison of well curves in time domain and inverted result at well location (CDP 37) for Young's modulus and Poisson ratio. From the inverted results, and we can see that the Young's modulus shows anomalously high value and Poisson ratio shows anomalously low value in the target reservoir at 1300 ms. This result is consistent with the drilling and rock physics analysis result.

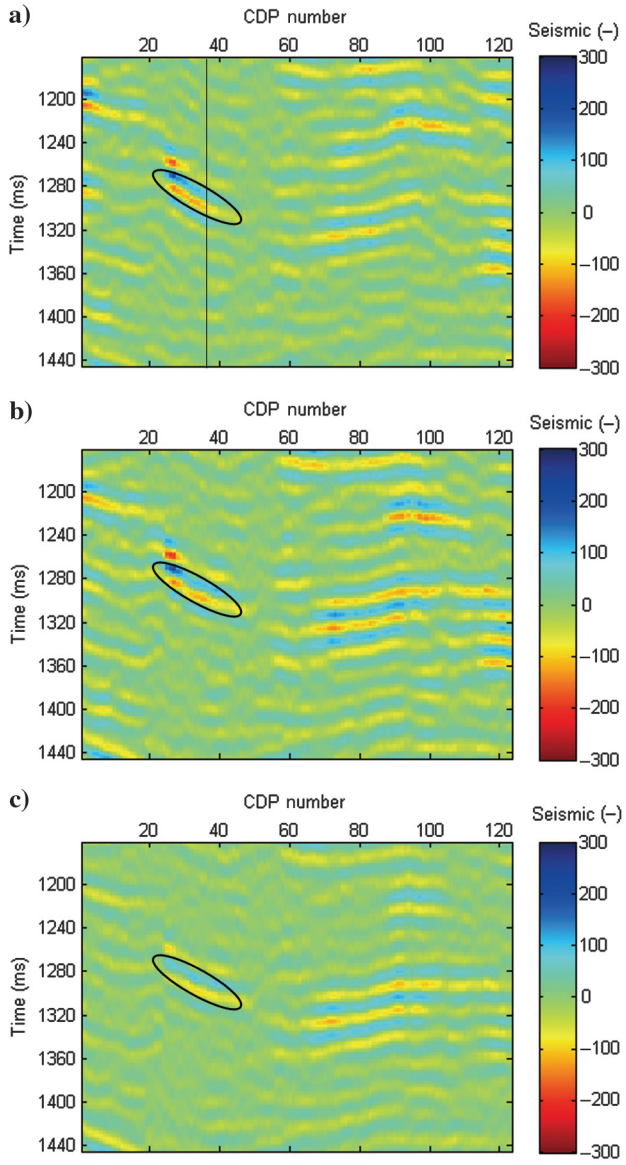

Figure 4. Angle-stack seismic profiles with different angle range (a) 10° (5°–15°), (b) 20° (15°–25°), and (c) 30° (25°–35°).

Downloaded 01/25/15 to 121.251.241.147. Redistribution subject to SEG license or copyright; see Terms of Use at http://library.seg.org/

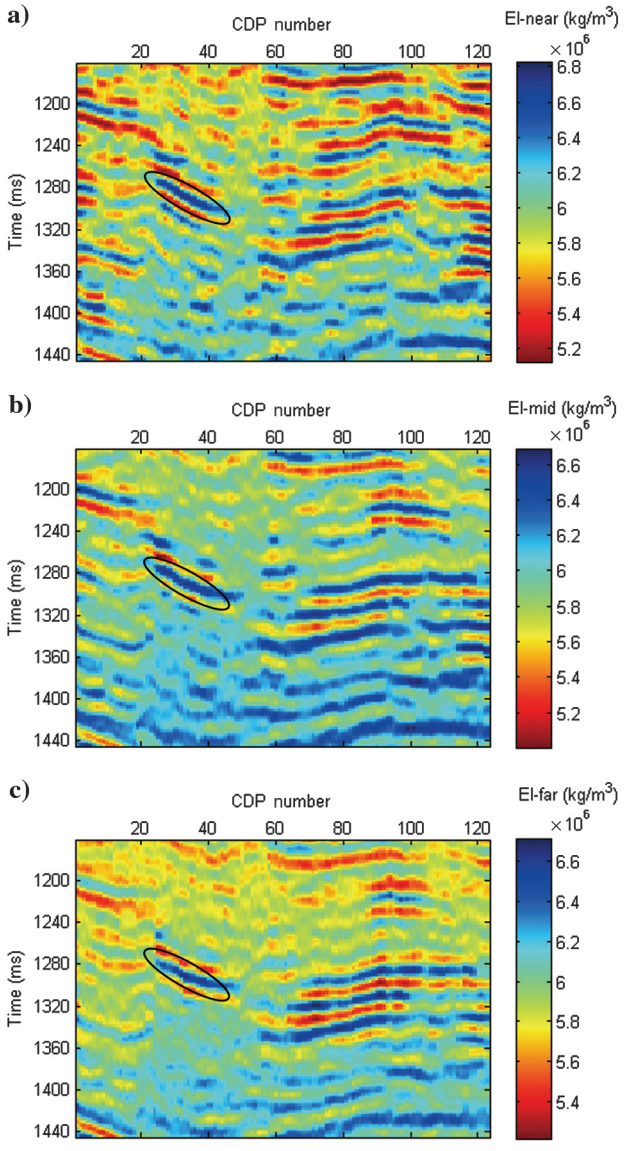

Figure 5. Elastic Bayesian inversion result with different angle range (a) 10° (5°–15°), (b) 20° (15°–25°), and (c) 30° (25°–35°).

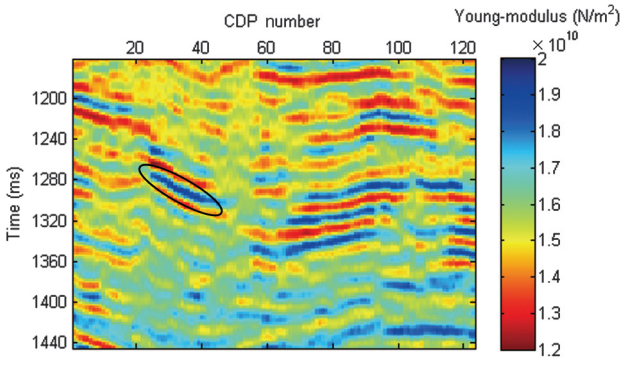

Figure 6. Profile of the inverted result of Young's modulus.

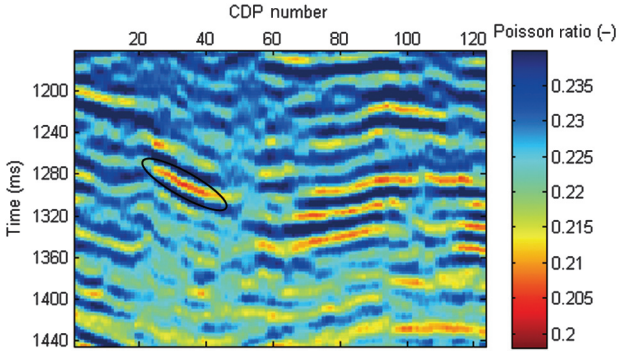

Figure 7. Profile of the inverted result of Poisson ratio.

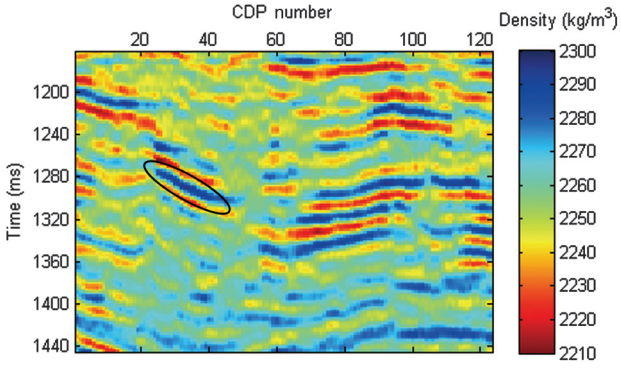

Figure 8. Profile of the inverted result of density.

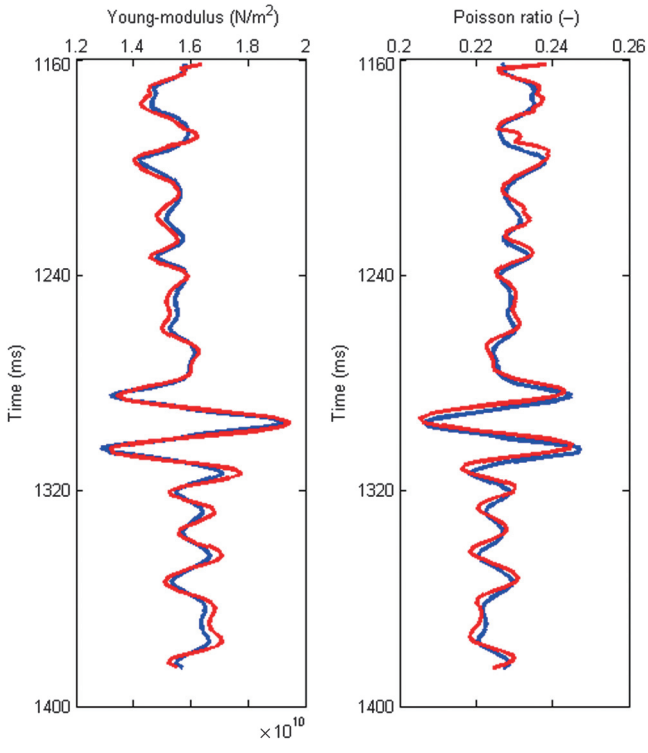

Figure 9. Comparison of well curves in time domain and inverted result at well location.

Downloaded 01/25/15 to 121.251.241.147. Redistribution subject to SEG license or copyright; see Terms of Use at http://library.seg.org/

CONCLUSIONS

We used the relationship among Young's modulus, Poisson ratio, P-wave and S-wave velocities, and density to reformulate the elastic equations in terms of Young's modulus, Poisson ratio, and density. With this formulation, the Young's modulus and Poisson ratio can be inverted directly without explicitly using the inverted density in the calculation of Young's modulus. The density is difficult to invert. Large angles of incidence and large offsets are needed to determine density through AVO inversion. The estimated density is more contaminated by noise than the estimated P-impedance reflectivity and S-impedance reflectivity. Our formulation of the elastic impedance equation estimated Young's modulus without explicitly using the inverted density, and we suggest that this formulation might minimize the effect of noise in the estimation of Young's modulus and Poisson ratio. Furthermore, to enhance the stability of estimating Young's modulus, Poisson ratio, and density from elastic impedances, we present a stable EVA-DSVD inversion approach with the novel elastic impedance equation in terms of Young's modulus, Poisson ratio, and density. The model and field test serve to confirm the validity of the proposed method.

ACKNOWLEDGMENTS

We would like to acknowledge the sponsorship of the National 973 Program of China (2013CB228604) and the National Grand Project for Science and Technology (2011ZX05030-004-002, 2011ZX05019-003 and 2011ZX05006-002) for funding this research. The first author acknowledges the support of the Australian and Western Australian Governments and the North West Shelf Joint Venture Partners, as well as the Western Australian Energy Research Alliance (WA:ERA) and Foundation from SINOPEC Key Laboratory of Geophysics (WTYJY-WX2013-04-01). We also thank the anonymous reviewers for their constructive suggestion.

REFERENCES

Aki, K., and P. G. Richards, 1980, Quantitative seismology, 2nd ed.: W. H. Freeman and Co.

Alemie, W., and M. D. Sacchi, 2011, High-resolution three-term AVO inversion by means of a Trivariate Cauchy probability distribution: Geophysics, **76**, no. 3, R43–R55, doi: 10.1190/1.3554627.

Arsalan, S. I., and A. Yadav, 2009, Application of extended elastic impedance: A case study from Krishna-Godavari Basin, India: The Leading Edge, **28**, 1204–1209, doi: 10.1190/1.3249775.

Cambois, G., 2000, AVO inversion and elastic impedance: 70th Annual International Meeting, SEG, Expanded Abstracts, 142–145.

Connolly, P., 1999, Elastic impedance: The Leading Edge, **18**, 438–452, doi: 10.1190/1.1438307.

Downton, J. E., 2005, Seismic parameter estimation from AVO inversion: Ph.D. thesis, University of Calgary.

Duffaut, K., T. Alsos, M. Landro, H. Rognø, and N. F. Al-Najjar, 2000, Shear-wave elastic impedance: The Leading Edge, **19**, 1222–1229, doi: 10.1190/1.1438510.

Fatti, J. L., G. C. Smith, P. J. Vail, and P. J. Strausset al., 1994, Detection of gas in sandstone reservoirs using AVO analysis: A 3-D seismic case history using the Geostack technique: Geophysics, **59**, 1362–1376, doi: 10.1190/1.1443695.

Goodway, B., T. Chen, and J. Downton, 1997, Improved AVO fluid detection and lithology discrimination using Lamé petrophysical parameters; "lambda rho","mu rho", & "lambda/mu fluid stack", from P and S inversions: 67th Annual International Meeting, SEG, Expanded Abstracts, 183–186.

Harris, N. B., J. L. Miskimins, and C. A. Mnich, 2011, Mechanical anisotropy in the Woodford Shale, Permian Basin: Origin, magnitude, and scale: The Leading Edge, **30**, 284–291, doi: 10.1190/1.3567259.

Lu, S., and G. A. McMechan, 2004, Elastic impedance inversion of multichannel seismic data from unconsolidated sediments containing gas hydrate and free gas: Geophysics, **69**, 164–179, doi: 10.1190/1.1649385.

Ma, J., and I. B. Morozov, 2005, The exact elastic impedance as a ray-path and angle of incidence function: 75th Annual International Meeting, SEG, Expanded Abstracts, 269–272.

Ma, J., and I. B. Morozov, 2006, A fluid detection study from Zoeppritz elastic impedance: 76th Annual International Meeting, SEG, Expanded Abstracts, 284–288.

Mallick, S., 2007, Amplitude-variation-with-offset, elastic-impedence, and wave-equation synthetics — A modeling study: Geophysics, **72**, no. 1, C1–C7, doi: 10.1190/1.2387108.

Mallick, S., , X. Huang, and J. Lauve et al., 2000, Hybrid seismic inversion: A reconnaissance tool for deepwater exploration: The Leading Edge, **19**, 1230–1237, doi: 10.1190/1.1438512.

Martins, J., 2002, An approach for elastic impedance in weakly anisotropic media: 72nd Annual International Meeting, SEG, Expanded Abstracts, 185–188.

Morozov, I. B., 2010, Exact elastic P/SV impedance: Geophysics, **75**, no. 2, C7–C13, doi: 10.1190/1.3318268.

Russell, B. H., D. Gray, and D. P. Hampson, 2011, Linearized AVO and poroelasticity: Geophysics, **76**, no. 3, C19–C29, doi: 10.1190/1.3555082.

Russell, B. H., K. Hedlin, F. J. Hilterman, and L. R. Lines, 2003, Fluid-property discrimination with AVO: A Biot-Gassmann perspective: Geophysics, **68**, 29–39, doi: 10.1190/1.1543192.

Sacchi, M. D., and T. J. Ulrych, 1995, High-resolution velocity gathers and offset space reconstruction: Geophysics, **60**, 1169–1177, doi: 10.1190/1.1443845.

Savic, M., , B. VerWest, R. Masters, and A. Sena et al., 2000, Elastic impedance inversion in practice: 70th Annual International Meeting, SEG, Expanded Abstracts, 689–692.

Sena, A., , G. Castillo, and K. Chesser et al., 2011, Seismic reservoir characterization in resource shale plays: "Sweet spot" discrimination and optimization of horizontal well placement: 81st Annual International Meeting, SEG, Expanded Abstracts, 1744–1748.

Shuey, R. T., 1985, A simplification of the Zoeppritz equations: Geophysics, **50**, 609–614, doi: 10.1190/1.1441936.

Thompson, P., , J. J. Hartman, and M. Anandito et al., 2009, Distinguishing gas sand from shale/brine sand using elastic impedance data and the determination of the lateral extent of channel reservoirs using amplitude data for a channelized deepwater gas field in Indonesia: The Leading Edge, **28**, 312–317, doi: 10.1190/1.3104077.

Wang, B., X. Yin, and F. Zhang, 2006, Lamé parameters inversion based on elastic impedance and its application: Applied Geophysics, **3**, 120–123, doi: 10.1007/s11770-006-0018-z.

Whitcombe, D. N., 2002, Elastic impedance normalization: Geophysics, **67**, 60–62, doi: 10.1190/1.1451331.

Zhang, S., X. Yin, and F. Zhang, 2009, Fluid discrimination study from fluid elastic impedance (FEI): 79th Annual International Meeting, SEG, Expanded Abstracts, 2437–2441.

Zong, Z., X. Yin, and G. Wu, 2011, Elastic impedance Bayesian inversion for Lamé parameters extracting: Oil Geophysical Prospecting (in Chinese), **46**, 598–604.

Zong, Z., X. Yin, and G. Wu, 2012, AVO inversion and poroelasticity with P- and S-wave moduli: Geophysics, **77**, no. 6, N17–N24, doi: 10.1190/geo2011-0214.1.